# Viable curvaton models from the $f_{\mathrm{NL}}$ parameter

L. F. Guimarães[1,2,*] and F. T. Falciano[1,3,†]

[1]*CBPF—Centro Brasileiro de Pesquisas Físicas, Xavier Sigaud Street 150, zip 22290-180, Rio de Janeiro, RJ, Brazil*

[2]*Dipartimento di Fisica, Università di Pisa and INFN, Sezione di Pisa, Largo Pontecorvo 3, I-56127 Pisa, Italy*

[3]*PPGCosmo, CCE—Universidade Federal do Espírito Santo, zip 29075-910, Vitória, ES, Brazil*

(Received 30 November 2020; accepted 10 March 2021; published 25 March 2021)

In this paper, we propose a method to reconstruct the curvaton potential from a scale-dependent non-Gaussianity parameter $f_{\mathrm{NL}}$. We exemplify our method, devising a weakly self-interacting curvaton model that produces a scale-dependent $f_{\mathrm{NL}}$ that crosses zero twice and is bounded from below and above. We identify the higher value of crossing with the cosmic microwave background (CMB) pivot scale, making the lower value fall within important structure formation scales. In addition, our curvaton model satisfies the observational constraints and leads to a $k$-dependent $f_{\mathrm{NL}}$ that can explain the CMB dipolar modulation. Our procedure can be straightforwardly extended to reconstruct the curvaton potential instead from the $g_{\mathrm{NL}}$ parameter.

DOI: 10.1103/PhysRevD.103.063530

## I. INTRODUCTION

Modern cosmology is based on a six-parameter model of the early Universe that has been tested with great precision by measuring the cosmic microwave background radiation (CMB) anisotropies. The latest Planck results [1–3] confirm the concordance model and provide accurate information on the cosmological parameters. In particular, the primordial density perturbations are consistent with Gaussian curvature perturbations, and the data are well suited to the inflationary scenario [4]. The power spectrum has a scalar spectral index of $n_s = 0.9649 \pm 0.0042$ and a small tensor-to-scalar ratio $r < 0.064$. The primordial non-Gaussianities have not yet been detected, but there are constraints for all types of shapes. In particular, the local shape is constrained to be $f_{\mathrm{NL}}^{\mathrm{local}} = -0.9 \pm 5.1$ [5].

Inflation offers a mechanism to explain the existence of the primordial cosmological perturbations. The most simple scenario is single-field inflation (SFI), where a scalar field follows a slow-roll dynamics and is simultaneously responsible for driving the almost exponential expansion of the Universe, and its density perturbations work as seeds for the CMB [6]. Thus, a slow-roll SFI model provides the observed Gaussian and almost scale-independent temperature fluctuations [7].

There are, however, at least two motivations to consider alternatives to SFI. In recent years, theoretical arguments indicate that the scenario might be not in the string theory landscape but in its swampland [8–11]. In addition, SFI is not suitable to address the CMB anomalies or observation of primordial non-Gaussianities. The CMB anomalies manifested on the Planck data [12] still have a low statistical significance of $3\sigma$. Nevertheless, the fact that they were measured by two different surveys, namely WMAP and then the Planck satellites, suggests that these anomalies might not be just a systematic error or foreground contamination, and if they exist, the statistical anomalies go against the cosmological principle [13,14].

SFI is not the unique successful scenario of the early Universe. There are two main alternative classes of models. First are the bouncing models, which also give an almost scale-invariant power spectrum with the correct redshift tilt and negligible production of gravitational waves [15–24]. Many bouncing models avoid constraints coming from the swampland conjectures, especially by the absence of a de Sitter expansion phase [25–27]. Another route is to preserve an inflationary phase, albeit not in a single-field slow-roll setting. Multifield inflation (MFI) models [28], in which there is more than one scalar field ruling the inflationary regime, could be a requirement for inflation to happen in the string theory landscape [29], while warm inflation provides alternative routes around the issues [30,31].

Among the MFI models, the curvaton models are simple extensions of SFI with the addition of only one extra scalar field [32,33]. In this scenario, the background dynamics is still driven by the inflaton, but the cosmological perturbations now come from the density fluctuations of the curvaton field. A distinct feature of these models is that

*lfog@cbpf.br
†ftovar@cbpf.br

 

the curvaton produces isocurvature perturbations instead of the common inflaton adiabatic perturbations. Only after the decay into radiation do the curvaton isocurvature modes turn into adiabatic ones, which then seed the CMB. This scenario alleviates the constraints on the inflaton field [34] while still producing the observed almost scale-invariant spectrum and the negligible amplitude of the primordial gravitational waves. Another advantage of this scenario is that it allows for large non-Gaussianities—indeed, much higher than in SFI.

A possible mechanism to account for the CMB anomalies is to consider non-Gaussian super-Hubble perturbations. A non-Gaussian mixing of long and short scale modes [35] breaks the perturbations' isotropy and can explain the hemispherical asymmetry [36–39]. In particular, the curvaton scenario predicts non-Gaussian primordial perturbations due to a quadratic dependence on the curvaton field in $\zeta$ [32].

The self-interacting models [40–42] are of particular interest, inasmuch as they provide scale-dependent non-Gaussianities that allow for the non-Gaussianity parameters $f_{\rm NL}$ and $g_{\rm NL}$ to vary by orders of magnitude between different scales. In this case, it is possible to have large non-Gaussianity at large scales and still satisfy the observational constraint on $f_{\rm NL}$. In addition, scale-dependence models can also modulate the non-Gaussianities and get the right amount of power asymmetry in the CMB [35,43,44].

In the present work, we show how to construct viable curvaton models from the properties of the $f_{\rm NL}$ parameter. In particular, due to the change of sign, we manage to have a $f_{\rm NL}$ close to zero at the observable scales but still have large non-Gaussianities away from the pivot scale. The paper is organized as follows: In Sec. II, we review the self-interacting curvaton scenario, and in Sec. III, we show how to construct curvaton models that implement the desired features of $f_{\rm NL}$. In Sec. IV, we analyze the parameter space of one such model and show that our procedure alleviates its fine-tuning. In Sec. V, we conclude with final remarks. Throughout the paper, unless explicitly written, we use Planck mass $M_{\rm Pl} = 1$.

## II. CURVATON SCENARIO

### A. Self-interacting curvaton scenario

The curvaton scenario goes beyond SFI by the addition of a second scalar field, dubbed the curvaton. Usually, this extra scalar field is minimally coupled to gravity and does not interact with the inflaton. The latter drives the background dynamics, while the curvaton produces the observed cosmological perturbations. There are also interactive models [45,46] where the potential has a cross term coupling the curvaton with the inflaton. These interactive models satisfy the observational constraints, but at the cost of increasing the number of free parameters of the model. Here, we shall consider only self-interacting curvaton models, which have scale-dependent non-Gaussianity [36], such that the Lagrangian reads

$$\mathcal{L}(\varphi,\sigma) = K(\varphi) + K(\sigma) + V(\varphi) + V(\sigma), \tag{1}$$

where $K(X)$ and $V(X)$ denote the kinetic and potential terms of the inflaton and curvaton fields, respectively. In contrast to SFI models, in the curvaton scenario, the inflaton has a negligible contribution to the cosmological perturbations due to a lower inflaton mass $m_\varphi$ as compared to the SFI models [47].[1] As a consequence, the magnitude of tensor perturbations is likewise negligible as compared to the SFI. Notwithstanding, the energy density of the curvaton is always subdominant and does not contribute to the background dynamics. It is the inflaton slow-roll regime that drives the almost exponential expansion of the Universe, while the curvaton follows its own evolution, which does not need to be frozen but can be a slow roll different from the inflaton dynamics.

As usual, reheating takes place at the end of the inflaton slow-roll regime, when it oscillates around the minimum of the potential with an equation of state $p = \omega\rho$ with $\omega \approx 0$. During this process, the inflaton decays into radiation. After decay, we are left with a reheated Universe, with energy density radiation-dominated.

In our scenario, the curvaton field follows a similar decay regime, albeit delayed in time. Thus, we consider potentials for the curvaton with a local minimum that can be approximated by a quadratic potential, and where the coherent oscillations makes the curvaton decay as pressureless dust.[2] In addition, we assume the sudden decay approximation in which the curvaton instantaneously decays into radiation when its decay rate equals the Hubble parameter[3]—i.e., $\Gamma_\sigma = H$.

During the inflationary phase, the curvaton produces only isocurvature perturbations. Due to thermal and chemical equilibrium, after the curvaton decay they are then converted into adiabatic perturbations. This conversion process was first proposed by Mollerach [50] and later applied to the curvaton scenario in Refs. [32,33]. The transfer of isocurvature perturbation into curvature perturbation can be described as [32]

$$\zeta \sim r_{\rm dec}\delta, \tag{2}$$

where $r_{\rm dec}$ and $\delta$ are the curvaton fractional energy density and the isocurvature perturbation, respectively, and $\zeta$ is the

[1]The scenario actually allows for both fields to contribute to cosmological perturbations [45,46].

[2]There are models in which the behavior of the potential at small values of the field is not quadratic; see Ref. [48] and references therein.

[3]It can be shown that the sudden decay is a good approximation for the exact gradual decay. Moreover, it does not have an impact on the primordial observables [49].

final adiabatic perturbation. The fractional energy density gives the curvaton contribution to the total energy density and reads

$$r_{\rm dec} = \left.\frac{3\rho_\sigma}{3\rho_\sigma + 4\rho_\gamma}\right|_{\rm dec} \sim \frac{V(\sigma_{\rm dec})}{3\Gamma^2}, \tag{3}$$

where $\rho_\sigma$ and $\rho_\gamma$ are the curvaton and the radiation density, respectively, at the time of the curvaton decay. During its reheating, the curvaton redshifts more slowly than radiation, since it behaves as dust; hence, if the curvaton decays long after the inflaton, the curvaton dominates the energy density of the Universe, and $r_{\rm dec} \sim 1$. On the other hand, if the decay happens shortly after the inflaton's decay, then $r_{\rm dec} \ll 1$, which means a large non-Gaussianity [see discussion after Eq. (11)]. Therefore, we assume that the curvaton decays not long after the inflaton, and hence $r_{\rm dec} \sim 10^{-2}$.

We can calculate the curvature perturbation by the $\delta N$ formalism [51]. The difference in the curvature perturbation equals the number of e-folds between the two hypersurfaces $\zeta \equiv \delta N$. Hence, for single-source curvaton models, we have

$$\zeta \approx N_{,\sigma}\delta\sigma + \frac{1}{2}N_{,\sigma\sigma}\delta\sigma^2 + \cdots,$$

where $N_{,\sigma}$ is the derivative of $N$ with respect to the curvaton field $\sigma$ at the initial hypersurface. The curvature perturbation power spectrum is defined as

$$\mathcal{P}_\zeta(k) = {N_{,\sigma}}^2 \mathcal{P}_s \approx \frac{r_{\rm dec}^2}{9\pi^2}\left(\frac{\sigma'_{\rm osc}}{\sigma_{\rm osc}}\right)^2 H_k^2 \tag{4}$$

where $\mathcal{P}_s(k) = H_k^2/(4\pi^2)$ is the scalar power spectrum for the mode $k$. We have that $\sigma_{\rm osc} = \sigma_{\rm osc}(\sigma_k)$ is the amplitude of the oscillations.[4] One can show that $N_{,\sigma} = \frac{2}{3} r_{\rm dec}(\sigma'_{\rm osc}/\sigma_{\rm osc})$. Therefore, the spectral index reads

$$n_s - 1 \approx 2\frac{\dot{H}_k^2}{H_k^2} + 2\frac{V_{,\sigma\sigma}}{3H_k^2} \approx -2\epsilon_H + 2\eta_\sigma. \tag{5}$$

Notwithstanding, the inflaton still gives important contributions, since it dominates the background dynamics. In the above equation, we define the slow-roll parameters as usual—namely,

$$\epsilon_H \equiv \frac{\dot{H}_k^2}{H_k^2}, \qquad \eta_\sigma \equiv \frac{V_{,\sigma\sigma}(t_k)}{3H_k^2}. \tag{6}$$

Even though the curvaton does not interact with the inflaton, the scalar perturbations and spectral index have contributions from both fields. The spectral index [Eq. (5)] has a leading contribution $\epsilon_H$, the inflaton slow-roll parameter. The curvaton $\eta_\sigma$, if positive, must be subleading and of order $10^{-2}$ or lower so that the spectrum is red and quasi-scale-invariant.[5] The tensor-to-scalar ratio $r$ is largely suppressed in the curvaton scenario as compared to SFI,

$$r = 16\epsilon_H \frac{\mathcal{P}_\varphi}{\mathcal{P}_\zeta} \approx 0 \ll r_{\rm SFI}, \tag{7}$$

where again we are dealing with the fact that the inflaton does not contribute to the perturbations $\mathcal{P}_\zeta \gg \mathcal{P}_\varphi$. One of the advantages of the curvaton scenario is to evade the need for $\epsilon_H \propto 1/N^2$ (for $N$ around 60 e-folds) in order to fit the current observational sensibility, $r < 10^{-2}$ [34]. Indeed, SFI models that lead to $\epsilon_H \propto 1/N$, such as chaotic inflation [6,52], can now be used as the inflaton component of the curvaton scenario, since they satisfy both constraints on $r$ and $n_s - 1$.

In order to quantify the amount of non-Gaussianity in the model, we can Taylor-expand the curvature perturbation $\zeta(k)$ in terms of its Gaussian component $\zeta_G$ as [53]

$$\zeta = \zeta_G + \frac{3}{5} f_{\rm NL}\zeta_G^2 + \frac{9}{25} g_{\rm NL}\zeta_G^3 + \mathcal{O}(\zeta_G^4). \tag{8}$$

By definition, the nonlinearity parameters $f_{\rm NL}$ and $g_{\rm NL}$ encode the non-Gaussianity from the second- and third-order terms, respectively. During the phase of coherent oscillations around the minimum of the potential, the energy density of the curvaton field for a mode $k$ can be approximated by $\rho_\sigma = m_\sigma^2\sigma_{\rm osc}^2/2$. Repeating the expansion to third order in the $\delta N$ formalism [53] gives

$$\begin{aligned}\zeta(k) = {} & \frac{2r_{\rm dec}}{3}\frac{\sigma'_{\rm osc}}{\sigma_{\rm osc}}\delta\sigma_k(t_k) \\ & + \frac{1}{9}\left[3r_{\rm dec}\left(1 + \frac{\sigma_{\rm osc}\sigma''_{\rm osc}}{{\sigma'_{\rm osc}}^2}\right) - 4r_{\rm dec}^2 - 2r_{\rm dec}^2\right] \\ & \times \left(\frac{\sigma'_{\rm osc}}{\sigma_{\rm osc}}\right)^2 \delta\sigma_k^2(t_k) \\ & + \frac{4}{81}\left[10r_{\rm dec}^4 + 3r_{\rm dec}^5 + \frac{9r_{\rm dec}}{4}\left(\frac{\sigma_{\rm osc}^2\sigma'''_{\rm osc}}{{\sigma'_{\rm osc}}^3} + 3\frac{\sigma''_{\rm osc}\sigma_{\rm osc}}{{\sigma'_{\rm osc}}^2}\right)\right. \\ & \left. - 9r_{\rm dec}^2\left(1 + \frac{\sigma_{\rm osc}\sigma''_{\rm osc}}{{\sigma'_{\rm osc}}^2}\right)\right]\left(\frac{\sigma'_{\rm osc}}{\sigma_{\rm osc}}\right)^3 \delta\sigma_k^3(t_k) + \mathcal{O}(\delta\sigma_k^4). \end{aligned} \tag{9}$$

Note that the nonlinearity parameters $f_{\rm NL}$ and $g_{\rm NL}$ are scale dependent. In order to have a scale-independent parameter, one needs $\sigma_{\rm osc}(\sigma_k)$ not to depend on $\sigma_{\rm k}$. Straightforward comparison of Eqs. (8) and (9) gives

[4]We prove that $\sigma_{\rm osc}$ depends on $\sigma_{\rm k}$ later in this same section.

[5]Models with negative spectral index would be preferred because of the requirement of a red spectrum, and would alleviate some conditions imposed on the inflaton, via $\epsilon_H$.

$$f_{\rm NL} = \frac{5}{4}\frac{f_{\rm osc}}{r_{\rm dec}} - \frac{5}{3} - \frac{5}{6}r_{\rm dec},$$
$$g_{\rm NL} = \frac{25}{24}\frac{g_{\rm osc}}{r_{\rm dec}^2} - \frac{25}{6}\frac{f_{\rm osc}}{r_{\rm dec}} - \frac{25}{12}\left(f_{\rm osc} - \frac{10}{9}\right) + \frac{125}{27}r_{\rm dec} + \frac{25}{18}r_{\rm dec}^2, \quad (10)$$

where

$$f_{\rm osc} \equiv 1 + \frac{\sigma_{\rm osc}\sigma''_{\rm osc}}{\sigma'^2_{\rm osc}}, \qquad g_{\rm osc} \equiv \frac{\sigma^2_{\rm osc}\sigma'''_{\rm osc}}{\sigma'^3_{\rm osc}} + 3\frac{\sigma''_{\rm osc}\sigma_{\rm osc}}{\sigma'^2_{\rm osc}}. \quad (11)$$

A prime in the above equations indicates derivatives with respect to $\sigma_k$. The terms proportional to $r_{\rm dec}^{-1}$ show that the faster the curvaton decays, the larger are the non-Gaussianities. In addition, the lower the cross section $\Gamma$, the longer it takes for the system to reach the sudden decay condition $H \sim \Gamma$. Note that to lower the value of the cross section means to reduce the magnitude of the curvaton interactions, and consequently also their fluctuations. Thus, higher $r_{\rm dec}$ values produce smaller magnitudes of fluctuation and smaller non-Gaussianities.

The curvaton dynamics is characterized by two distinct regimes. The first is the slow-roll regime of the curvaton, given by

$$3H\dot{\sigma} + m_\sigma^2\sigma + V^{\rm SI}_{,\sigma}(\sigma) \approx 0, \quad (12)$$

where $V^{\rm SI}(\sigma)$ is the self-interacting part of the potential.[6]

The solution for the slow-roll regime $\sigma_{\rm SR}$ is a nonlinear function of $\sigma_{\rm k}$. We assume that it is valid until the time $t_q$, when the curvaton reaches its second regime. There, the curvaton oscillates around its quadratic minimum, and the self-interactions are no longer important. This is known as a coherent oscillating phase, whose dynamics reads

$$\ddot{\sigma} + 3H\dot{\sigma} + m_\sigma^2\sigma \approx 0. \quad (13)$$

The solution for this stage is of the form $\sigma(t) = \sigma_{\rm osc} f_{\rm inf}(t)$, where $f_{\rm inf}$ is a function dependent only on the background dynamic given by the inflaton; see Refs. [36,54]. We suppose an instantaneous transition between the slow-roll and the coherent oscillation regimes and match the respective solutions, which allows us to write $\sigma_{\rm osc} = \beta\sigma_{\rm SR}(t_q)$, where $\beta$ is a constant parameter. Therefore, $\sigma_{\rm osc}$ is proved to be dependent on $\sigma_{\rm k}$ as well.

We are interested in a particular set of self-interaction curvaton models, where the $\sigma_{\rm k}$ dependence on $\sigma_{\rm osc}$ is input by hand in order to better fit observational results. In the next section, we show how recent observations suggest the behavior needed for $f_{\rm NL}$, and, consequently, $\sigma_{\rm osc}(\sigma_{\rm k})$.

[6]The quadratic mass term emerges only in the small field value limit, hence it is absent in Eq. (12). However, the Taylor expansion of the total potential $V$ around its minimum makes the mass term reappear in Eq. (13).

## III. CONSTRUCTING VIABLE MODELS FROM $f_{\rm NL}$

The Planck Collaboration [2] showed that the strength of the non-Gaussian signal for $f_{\rm NL}$ does not go beyond order unity, indicating that primordial non-Gaussianities are seemingly very small. A way out of this constraint is to consider scale-dependent non-Gaussianity models, in order to have large values of $f_{\rm NL}$ away from the observed scales (in particular, away from the pivot scale used for the CMB maps). Models with a change of sign in $f_{\rm NL}$, so that it remains close to zero over a limited range of wave numbers, can be adjusted to satisfy the present observational constraints. Evidently, such a range of wave numbers must be identified with the CMB scales which constrain the free parameters of the models. This procedure allows us to study how much fine-tuning is required to fit the observational data. The scale-dependent models are particularly interesting when one needs high values of non-Gaussianities—for instance, to account for the CMB anomalies [36–38]. In the following, we analyze how to construct models with a change of sign in the $f_{\rm NL}$ parameter and the effects this has on the dynamics of the curvaton field.

### A. Crossing $f_{\rm NL}$ parameter

In the literature, the non-Gaussianity parameter $f_{\rm NL}$ is typically parametrized as a power law given by

$$f_{\rm NL}(k) = f^0_{\rm NL}\left(\frac{k}{k_0}\right)^{n_{f_{\rm NL}}}, \quad (14)$$

where $f^0_{\rm NL}$ is the amplitude at a given pivot scale $k_0$, and the index $n_{f_{\rm NL}}$ is a constant [55,56]. However, this parametrization is no longer valid if $f_{\rm NL}$ crosses zero—namely, if it changes sign [36]. As we present in Sec. IV B, a better-suited parametrization allows for multiple changes in sign.

We can find the value of $\sigma_{\rm osc}$ in terms of $\sigma_k$ where the change of sign happens. The rhs of Eq. (11) shows that

$$f_{\rm osc} = \frac{(\sigma^2_{\rm osc})''}{2\sigma'^2_{\rm osc}} = 0 \Rightarrow (\sigma^2_{\rm osc})'' = 0. \quad (15)$$

The conditions for $f_{\rm osc}$ and $f_{\rm NL}$ to cross zero are different. Nevertheless, for $r_{\rm dec} \sim 0.05$, the values of the last two terms on the rhs of Eq. (10) are of order unity. The crossing is still guaranteed as long as the scale dependence of $f_{\rm NL}$ is strong enough. Thus, instead of the crossing of $f_{\rm NL}$, we consider the condition for $f_{\rm osc} = 0$. Equation (15) implies that the crossing is an extremal point for

$$(\sigma_{\rm osc}^2)' = 2\sigma_{\rm osc}\sigma'_{\rm osc}. \tag{16}$$

The function $\sigma_{\rm osc}$ is assumed to be a monotonic function of $\sigma_{\rm k}$, and the derivative $\sigma'_{\rm osc}$ must not cross zero; otherwise $f_{\rm osc}$ diverges. Moreover, the value of $k$ at the crossing of $f_{\rm osc}$ differs from the extreme of $\sigma'_{\rm osc}$ due to the factor $\sigma_{\rm osc}$. As a fact, at the extremal of $\sigma'_{\rm osc}$ we have $\sigma''_{\rm osc} = 0$, which means $f_{\rm osc} = 1$ instead of 0. Notwithstanding, it suffices that $\sigma'_{\rm osc}$ has one extremal point for Eq. (15) to be satisfied and, given the scale-dependence of the system, we expect that the values of $k$ for these two conditions should be close.

In summary, the function $\sigma_{\rm osc}$ is monotonic, and $\sigma'_{\rm osc}$ has an extremal point, but it is never zero; hence it is always positive or negative. The function $\sigma''_{\rm osc}$ does change sign at least once and must vary enough to guarantee that $f_{\rm NL}$ also changes sign. There are different ways in which one can implement these features. In the next section, we show one way to construct the curvaton potential in order to have exactly this kind of behavior. We study the parameter space of the model by combining the observational data with the conditions on $\sigma_{\rm osc}$ and its derivatives.

### B. Constructing the curvaton potential

The non-Gaussianity parameters depend basically on the relation $\sigma_{\rm osc}(\sigma_k)$—i.e., on how $\sigma_{\rm osc}$ is written in terms of $\sigma_k$. And to find $\sigma_{\rm osc}(\sigma_k)$, we need to solve the two regimes in Eqs. (12) and (13), hence different curvaton potentials result in different relations. Our goal is to be able, given a functional form $\sigma_{\rm osc}(\sigma_k)$, to specify the potential that after solving the dynamical equations will produce the desired $\sigma_{\rm osc}(\sigma_k)$.

We start by separating the slow-roll regime of the curvaton into two steps. We assume that when the value of the curvaton field is close to $\sigma_{\rm osc}$, the potential is close to quadratic and remains so until the minimum of the potential at the origin $\sigma = 0$. This guarantees the validity of the results from the conventional self-interaction curvaton scenario (Sec. II A).

Recall that $\sigma_{\rm q} \equiv \sigma(t_q) \propto \sigma_{\rm osc}$, and away from $\sigma_{\rm q}$, we need to consider the full expression of the potential—in particular, for the evolution around the observable scales $\sigma_{\rm k}$. Solving the slow-roll equation for these two regimes gives

$$\int_{\sigma_{\rm k}}^{\sigma_{\rm q}} \frac{{\rm d}\sigma}{\bar{V}_{,\sigma}} \sim \int_{\sigma_{\rm k}}^{\sigma_*} \frac{{\rm d}\sigma_{\rm q}}{\bar{V}_{,\sigma}} + \int_{\sigma_*}^{\sigma_{\rm q}} \frac{{\rm d}\sigma}{\sigma} = -\bar{\eta}_\sigma \mathcal{I}(t_q, t_k), \tag{17}$$

where $\bar{V} \equiv V/m_\sigma^2$, and $\sigma_*$ is the field value where we apply the matching condition to connect the slow-roll dynamics to the quadratic local minimum regime. Note that $\sigma_*$ cancels from the final expression, since it is evaluated where both solutions are equal, and hence is irrelevant. Following Ref. [36], in Eq. (17), we have defined

$$\mathcal{I}(t_q, t_k) \equiv H_k^2 \int_{t_k}^{t_q} \frac{{\rm d}t}{H(t)}, \qquad \bar{\eta}_\sigma = \frac{m_\sigma^2}{3H_k^2}. \tag{18}$$

Given an appropriate choice of $t_q$, the integral during the curvaton slow-roll regime gives $\mathcal{I}(t_q, t) \approx 1/\bar{\eta}_\sigma$. Thus, for values of $t \ll t_q$, the rhs of Eq. (17) equals $-\bar{\eta}_\sigma \mathcal{I} \approx -1$, and we can consider this term independent of $\sigma_k$. Close to $\sigma_q$, we have

$$\int \frac{{\rm d}\sigma}{\bar{V}_{,\sigma}} = \log[\sigma]. \tag{19}$$

Now, we assume that the potential is such that the integral containing $\bar{V}_{,\sigma}^{-1}$ admits a primitive function $G(\sigma)$, namely

$$\int_{\sigma_{\rm k}}^{\sigma_{\rm q}} \frac{{\rm d}\sigma}{\bar{V}_{,\sigma}} \sim G(\sigma_{\rm q}) - G(\sigma_{\rm k}), \tag{20}$$

and Eq. (17) can be recast as

$$G(\sigma) = \log\left[\sigma_{\rm osc}(\sigma)\right] + \text{terms independent of } \sigma_k. \tag{21}$$

To find the potential, we can invert Eq. (20) and write

$$V(\sigma) = m_\sigma^2 \int {\rm d}\sigma \frac{\sigma_{\rm osc}}{\sigma'_{\rm osc}}, \tag{22}$$

where $\sigma_{\rm osc}$ should be understood as the function $\sigma_{\rm osc}(\sigma)$ with the same functional form as $\sigma_{\rm osc}(\sigma_k)$. Given a physically motivated ansatz $\sigma_{\rm osc}(\sigma_k)$, integration of Eq. (22) gives the potential satisfying the slow-roll dynamics that produces the desired non-Gaussianity encoded in $\sigma_{\rm osc}(\sigma_k)$. By construction, the slow-roll solution is approximately $G(\sigma)$. This allows us to compute the curvaton slow-roll parameters and compare them with the observation of the primordial power spectrum. Moreover, using Eq. (10), we can also compute the non-Gaussianity parameters $f_{\rm NL}$ and $g_{\rm NL}$ of the model.

### C. Observables from the reconstruction

Similarly to what we have done for $f_{\rm NL}$, we can write the derivatives of the potential, namely the slow-roll parameters, in terms of $\sigma_{\rm osc}$ and its derivatives. Using Eq. (22), we have

$$V_{,\sigma} = m_\sigma^2 \frac{\sigma_{\rm osc}}{\sigma'_{\rm osc}}, \tag{23}$$

$$V_{,\sigma\sigma} = m_\sigma^2 \left(1 - \frac{\sigma_{\rm osc}\sigma''_{\rm osc}}{\sigma'^2_{\rm osc}}\right). \tag{24}$$

Comparing the above expression with the definition of $f_{\rm osc}$, Eq. (11), one immediately sees that

$$f_{\rm osc} + \frac{V_{,\sigma\sigma}}{m_\sigma^2} = 2. \tag{25}$$

It is worth remarking that the above expression is independent of the solution $\sigma_{\rm osc}$. Since $f_{\rm osc} = 1$ for $\sigma''_{\rm osc} = 0$, Eq. (25) shows that $V_{,\sigma\sigma} = m_\sigma^2$ at this point as well. We also conclude that

$$\begin{aligned}\eta_\sigma &= \frac{m_\sigma^2(2 - f_{\rm osc})}{3H_k^2} \\ &= 2\bar{\eta}_\sigma - \frac{4r_{\rm dec}\bar{\eta}_\sigma}{5}\left(f_{\rm NL} + \frac{5}{3} + \frac{5r_{\rm dec}}{6}\right);\end{aligned} \tag{26}$$

hence, for any model from our procedure, the parameter $\eta_\sigma$ can be written in terms of $\bar{\eta}_\sigma$ and $f_{\rm NL}$. Equation (26) generalizes the relation presented in Ref. [57], since it is still valid for large values of $f_{\rm NL}$ and $\eta_\sigma$. We see that in our scenario, there is an additional expression relating $f_{\rm NL}$, $\eta_\sigma$, and $H_k$. Note also that we can recover the condition $\eta_\sigma = 2\bar{\eta}_\sigma$ from Ref. [36], if $f_{\rm NL}(k_0) = -5/3 - 5r_{\rm dec}/6$.

In Sec. III A, we associated the change of sign in $f_{\rm osc}$ with the second derivative of $\sigma''_{\rm osc}$ being zero somewhere along the curvaton trajectory. Now, using Eq. (25), we conclude that the potential must also have an inflection point—i.e., $V_{,\sigma\sigma} = 0$. The inflection point, like for $f_{\rm osc}$, is not located where $\sigma''_{\rm osc} = 0$.

### D. Reconstructing a polynomial potential

The quartic and higher-power polynomial models have been studied in the literature [36,41,42,54]. Despite producing scale-dependent non-Gaussianities, these models predict high values of $\eta_\sigma$ over the region of low $f_{\rm NL}$. Therefore, such models are not favored by the Planck satellite results. Our goal here is to use them only as an example to show how our procedure works. In the next section, we shall deal with fitting the model to observations. For a polynomial potential of the form $V(\sigma) = \frac{1}{2}m^2\sigma^2 + \lambda\sigma^n$ with $n > 2$, the curvaton slow-roll solution is given by

$$\sigma_{\rm osc}(\sigma_{\rm k}) = \frac{\sigma_{\rm k}}{[e^{n-2} + (ne^{n-2} - n)\lambda\sigma_{\rm k}^{n-2}]^{1/(n-2)}}. \tag{27}$$

Using Eq. (27) as the ansatz for the procedure of Sec. III B, we obtain a potential given by

$$V(\sigma) = \frac{1}{2}m^2\sigma^2 + \lambda_{\rm eff}\sigma^n \quad \text{with} \quad \lambda_{\rm eff} = \lambda(1 - e^{-n+2}). \tag{28}$$

We see that the reconstruction gives a lower value for the coupling constant. The worst case is for $n = 3$, where $\lambda_{\rm eff} \approx 0.6321\lambda$ but already increases to $\lambda_{\rm eff} \approx 0.865\lambda$ for $n = 4$. The higher the power of the self-interaction, more precise is the reconstruction. This kind of shift in our reconstruction procedure does not change the qualitative behavior of our model, but it can change some observational scales such as the pivot value at which the non-Gaussianity parameter $f_{\rm NL}$ changes sign. The important point is that any feature input in the ansatz will also be present in the solutions derived by using the reconstructed potential; hence, the consistency of the procedure is guaranteed.

## IV. LINEARLY ACCELERATED MODELS

In Sec. III A, we described the main features that a solution $\sigma_{\rm osc}(\sigma_{\rm k})$ must have in order to produce a viable curvaton model with a change of sign in $f_{\rm NL}$. A possible realization of these conditions is for $\sigma''_{\rm osc}(\sigma_{\rm k})$ to be a linear function of $\sigma_{\rm k}$. Therefore, we consider an ansatz of the form

$$\sigma_{\rm osc} = a\sigma + \frac{1}{2}b\sigma^2 + \frac{1}{6}c\sigma^3, \tag{29}$$

where $a$, $b$, and $c$ are the free parameters of the solution. Applying the construction procedure of the last section, we arrive at the potential

$$\begin{aligned}\frac{V(\sigma)}{m^2} = V_0 + \frac{b}{3c}\sigma + \frac{\sigma^2}{6} - V_{\rm lg}\log(2a + 2b\sigma + c\sigma^2) \\ + V_{\rm arc}\arctan\left(\frac{b + c\sigma}{\sqrt{-b^2 + 2ac}}\right),\end{aligned} \tag{30}$$

where the two coefficients $V_{\rm lg}$ and $V_{\rm arc}$ are given in terms of the free parameters as

$$V_{\rm lg} = \frac{b^2 - 2ac}{3c^2}, \qquad V_{\rm arc} = \frac{4b(b^2 - 3ac)}{6c^2\sqrt{2ac - b^2}}. \tag{31}$$

The argument of the arctan has the same structure as the ansatz acceleration—i.e., $\sigma''_{\rm osc} = (b + c\sigma)$. Therefore, the inflection point for this term happens where the acceleration is zero, $\sigma_z = -b/c$. However, for the total potential [Eq. (30)], the inflection point is shifted away from $\sigma_z$ due to the presence of the other (subleading) terms.

In order to reduce the number of free parameters and simplify the analysis of the parameter space, we shall fix $a = 1/e$, which gives the quadratic curvaton solution in the limit $b = c = 0$. Note also that we have implicitly assumed $\sigma_{\rm osc}(0) = 0$. The ansatz is constructed to facilitate the study of the curvaton slow-roll solution and its resulting $f_{\rm NL}$ parameter. Therefore, it is convenient to discuss the model parameter space in terms of $b$ and $c$ and not in terms of the coefficients of the potential, because the former are directly connected to the non-Gaussianity parameters $f_{\rm NL}$ and $g_{\rm NL}$.

The first constraint on $b$ and $c$ comes from the change of sign of $\sigma''_{\rm q}(\sigma_{\rm k})$, which should happen during the curvaton slow roll. Therefore, the point $\sigma = -b/c$ should be smaller than the initial value of the field $\sigma_{\rm ini.} \equiv \sigma_{\rm max}$. That is represented by the black dotted lines in Fig. 1. This also implies that $b$ and $c$ must have opposite signs, inasmuch as $\sigma > 0$ during the slow roll.

The derivative $\sigma_{\rm q}'$ should not vanish anywhere; otherwise, both $f_{\rm NL}$ and $g_{\rm NL}$ diverge. Therefore, the models have a positive minimum for $\sigma_{\rm q}'$—i.e., we must have $b > -\sqrt{2c/e}$—that gives the red dashed line a constraint in Fig. 1. Note that this condition also avoid divergences in the potential [Eq. (30)]. Also, $\sigma_{\rm q}$ is a monotonically increasing function of $\sigma_{\rm k}$, since its derivative is always positive.

In addition, the log term of Eq. (30) has an argument proportional to $\sigma_{\rm osc}'$; hence we must also avoid $\sigma_{\rm q}' = 0$. As a consequence, we must exclude negative values of $c$—i.e., $c > 0$.

The curvaton field should always be positive during the slow roll; therefore $\sigma_{\rm q} > 0$, resulting in the blue dotted line in Fig. 1. This condition is, however, less strict and does not contribute, since it is always below the red line.

The last constraint comes from the condition on the curvaton evolution. We want the field to move towards the minimum of the potential at $\sigma = 0$, hence $\sigma_{\rm q}$ should never be greater than $\sigma_{\rm k}$, which gives the purple dash-dotted curve in Fig. 1. To sum up, the system of constraints reads

$$\begin{aligned}
&\text{if} \quad 0 < c < \frac{2}{\sigma_{\rm max}^2}, \quad -c\sigma_{\rm max} < b < 0;\\
&\text{if} \quad \frac{2}{\sigma_{\rm max}^2} < c < \frac{6e-6}{\sigma_{\rm max}^2}, \quad -\sqrt{2c} < b < 0;\\
&\text{if} \quad \frac{6e-6}{\sigma_{\rm max}^2} < c < c_{\rm max}, \quad -\sqrt{2c} < b < \frac{2e-2}{\sigma_{\rm max}} - \frac{1}{3}c\sigma_{\rm max};\\
&\text{where} \quad c_{\rm max} \equiv \frac{3}{\sigma_{\rm max}^2}(1+2e+\sqrt{12e-3}).
\end{aligned} \tag{32}$$

As a result, we conclude that the higher the value of $\sigma_{\rm max}$, the smaller the allowed parameter region for $(b, c)$. In other words, low values of $\sigma_{\rm max}$ alleviate the possible fine-tuning of models.

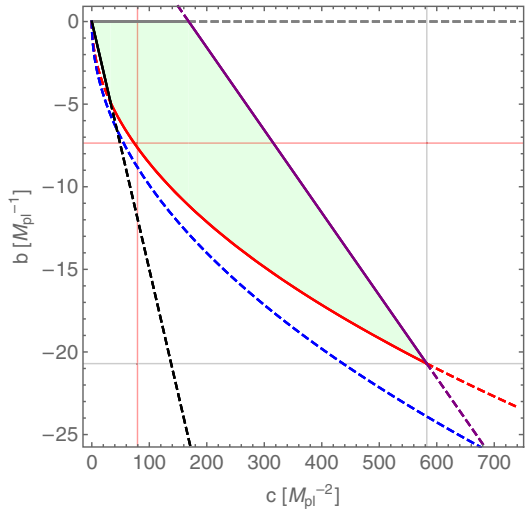


FIG. 1. Final allowed region for $b$ in green, when $\sigma_{\rm max} = 0.15$, $c > 0$, including all constraints. The red grid lines indicate the point $(b, c) = (-20/e, 216/e)$ for the model in Sec. IV A.

### A. Example A: $b = -20/e$, $c = 216/e$

In order to show the behavior of the non-Gaussianities parameter, in this section we study a concrete example by fixing $b = -20/e$ and $c = 216/e$. These values are well within the allowed parameter region (see Fig. 1), and they make the difference between the value $\sigma_{\rm q}'' = 0$ for the ansatz and that for the reconstructed solution small. Notice that these values of $b$ and $c$ extrapolate the current observational limits of $f_{\rm NL}$ and $g_{\rm NL}$ (see Ref. [5] and Fig. 6). However, they are suitable for studying the main features of the model. In Sec. V, we discuss the observational constraints of $b$ and $c$. Let us first compute the curvaton potential [Eq. (30)]. To determine the value of $V_0$, we require that $V(0) = 0$—i.e.,

$$V_0 \equiv \frac{2b(3c-b^2)}{3c^2\sqrt{2c-b^2}}\tan^{-1}\left(\frac{b}{\sqrt{2c-b^2}}\right) - \frac{\log 2}{3c^2}(2c-b^2), \tag{33}$$

which gives $V_0 \sim 0.016$ for the chosen values of the parameters. The Taylor expansion of the potential (30) at $\sigma = 0$ reads

$$V(\sigma) = \frac{m^2\sigma^2}{2} - b\frac{m^2\sigma^3}{6} + \mathcal{O}(\sigma^4), \tag{34}$$

confirming that indeed the potential can be approximated by a quadratic potential close to the origin. In Fig. 2, we show the results of our procedure. The top panel of Fig. 2 displays the potential constructed from the ansatz [Eq. (29)], while in the bottom panel we compare three solutions: the one coming from the reconstructed potential, the original ansatz, and the solution for the quadratic potential $V(\sigma) = m^2\sigma^2/2$.

Note that the field solution has no maximum or minimum, which guarantees that its velocity is never zero as constructed. The non-Gaussianity parameter $f_{\rm NL}$ is computed in the top panel of Fig. 3. The shape of the original ansatz and the reconstructed solution agree, but with a small difference in the amplitude. Therefore, we managed to recreate the behavior for $f_{\rm NL}$ as desired. The agreement between the two results grows[7] the closer the choice of parameters is to $b = -\sqrt{2c}$; see Fig. 4. However, such a choice also implies stronger non-Gaussianity and running $n_{f_{\rm NL}}$, beyond the most recent results.

Figure 3 also shows the behavior of the $g_{\rm NL}$ parameter in the bottom panel. It has an extreme at $\sigma_{\rm osc}'' = 0$, and since

[7]The results become more alike as the point of their change of sign tends toward $-b/c$.

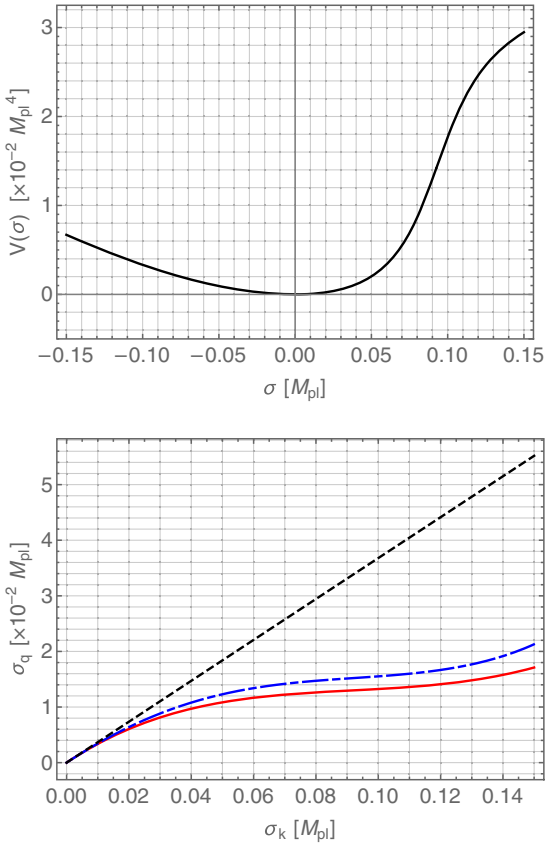


FIG. 2. Top: curvaton potential $V(\sigma)$ for example A, where $b = -20/e$, $c = 216/e$. The inflection point is located at $V_{\sigma\sigma} = 0$. Bottom: reconstructed (blue dash-dotted line), ansatz (red solid line), and quadratic potential (black dashed line) solutions for the curvaton slow-roll equation results in terms of $\sigma_{\rm k}$.

the first term of Eq. (11) dominates, it has $\sigma'''_{\rm osc}$ constant at the extreme. Note that with our choice of parameters, the magnitude of the $g_{\rm NL}$ is close to the current observational limit, which is $g_{\rm NL} \approx 5 \times 10^5$.

The authors of Ref. [57] analyze the relation between the features in the curvaton potential and a large running of the scalar spectral index. However, they make no explicit connection between features and the change of sign of $f_{\rm NL}$ and $\eta_\sigma$, as in Sec. III C. For our model, recalling Eq. (26), we have

$$\eta_\sigma = \frac{2m_\sigma^2}{3H_\kappa^2} - \frac{4r_{\rm dec}}{5}\bar{\eta}_\sigma\left(f_{\rm NL} + \frac{5}{3} + \frac{5r_{\rm dec}}{6}\right). \tag{35}$$

The CMB constrains $\eta_\sigma$ to be of order $10^{-2}$ where $f_{\rm NL}$ changes sign, but the former also depends on the inflationary scale. In turn, to constrain the value of $H_k$, we need to evaluate the spectral index and the amplitude of the perturbations [Eq. (4)]. In fact, we should also include the physics of the reheating [48]. Therefore, in the present analysis we will not fix $H_k$. To circumvent this issue, we plot $f_{\rm NL}$ together to $V_{,\sigma\sigma}$. As argued in Sec. III C and

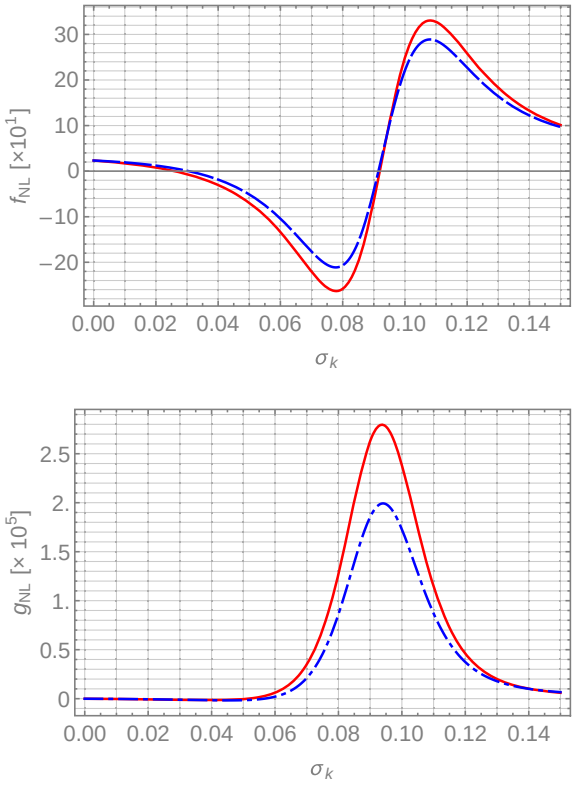


FIG. 3. Top: reconstructed $f_{\rm NL}$ (dash-dotted) parameter for example A in comparison to the ansatz (solid) with $b = -20/e$ and $c = 216/e$. Bottom: the same for $g_{\rm NL}$.

also in Ref. [57], for large values of $f_{\rm NL}$ we have $f_{\rm NL} \propto -\eta_\sigma$.

We show that a feature on $V(\sigma)$ induces a change of sign in $\sigma''$—i.e., a feature on the solution $\sigma_{\rm q}(\sigma_{\rm k})$. The converse is also true: if we start with an ansatz in which $\sigma'' = 0$ somewhere, there will be a change of sign in the reconstructed $V_{,\sigma\sigma}$. The same goes for $f_{\rm NL}$. We conclude that features are shared by these different observables.

We have also already demonstrated that the change of sign for the ansatz $f_{\rm osc}$ and $V_{,\sigma\sigma}$ happens in different scales.

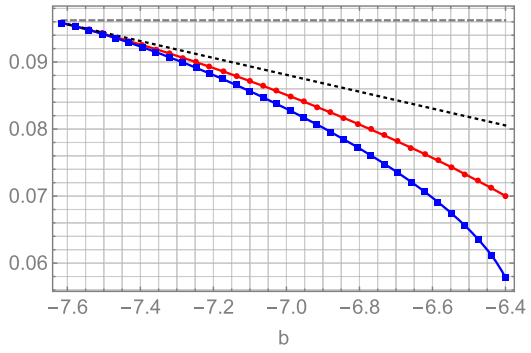


FIG. 4. Numerically computed zeros of $f_{\rm osc}$, as a function of $b$, from ansatz (red, circle) and reconstructed (blue, square) solutions. The ratio $-b/c$ is the black dotted line, while the ratio $b = -\sqrt{2c/e}$ is the gray dashed line. $c = 216/e$.

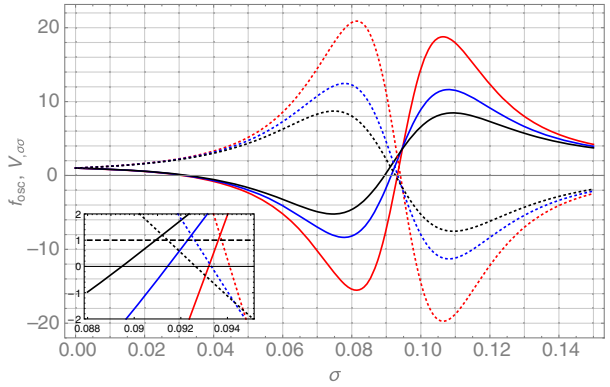


FIG. 5. Reconstructed $f_{\rm osc}$ (solid lines) and $V_{\sigma\sigma}$ (dotted lines) for varying $b$, $a = 1/e$, and $c = 216/e$. Their magnitudes grow with $|b|$. The distance between the crossing position decreases with growing $|b|$ for the chosen parameter range. In the highlight, we show the point where both are equal, which happens for a value a bit above $V_{\sigma\sigma} = 1$.

In Fig. 5, we show that, even for the reconstructed $f_{\rm osc}$, the zeroes of those functions are symmetric around the point where $f_{\rm osc} = V_{,\sigma\sigma}$. For $f_{\rm osc}$, the zero is located before $\sigma = -b/c$, while for the second derivative of the potential it happens after this value. We can also see what is indicated in Eq. (26): when we choose the pivot scale to be where $f_{\rm NL} = 0$, we have $\eta > 0$.

### B. Scale-dependence effects and CMB anomalies

The scale dependence of $f_{\rm NL}$ can be explicitly written by expanding the integral $\mathcal{I}(t_q, t_k)$ [see Eq. (18)] in terms of $\log(k/k_0)$. The pivot scale $k_0$ is defined as the value at which $f_{\rm NL} = 0$. Near the pivot scale, we have

$$\mathcal{I} = \log(k/k_0)[1 + \epsilon_0 \log(k/k_0)], \tag{36}$$

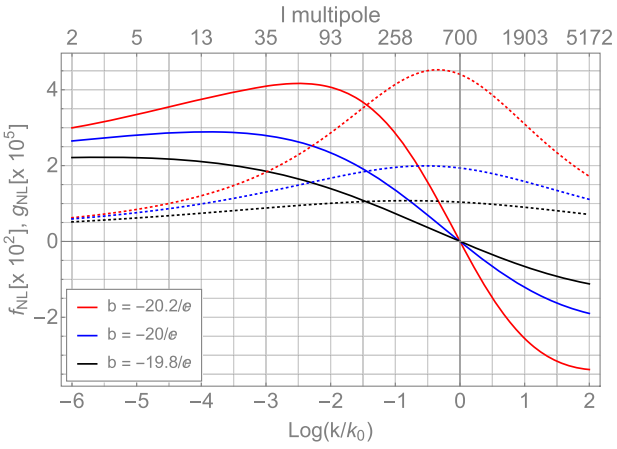


FIG. 6. Non-Gaussianity parameters $f_{\rm NL}$ (solid lines) and $g_{\rm NL}$ (dotted lines) for the model example A. We vary $b$ by $\pm 10\%$. The slow-roll parameters were chosen as $\epsilon_0 = 1/128$ and $\bar{\eta}_\sigma = 0.01$. $k_0$ is the pivot scale 0.05 Mpc$^{-1}$, defined as the scale at which $f_{\rm NL} = 0$.

where $\epsilon_0$ is the inflationary first slow-roll parameter at the pivot scale. Note that this modification makes $f_{\rm NL}$ depend on $\bar{\eta}_\sigma$ as well. The reconstructed solution for $f_{\rm NL}$ and $g_{\rm NL}$ can then be written in terms of $\log(k/k_0)$; see Fig. 6 below. Differently from Eq. (14), around the pivot scale for our model, the $f_{\rm NL}$ parameter is best described by a log parametrization; see Ref. [36].

As we vary the parameters $b$ and $c$, we see that the scale dependence of both nonlinear parameters changes. Higher values of $|b|$ enhance the non-Gaussianities of the scalar perturbations. On the other hand, higher values of $c$ result in lower values for $f_{\rm NL}$ and $g_{\rm NL}$. We illustrate the behavior for variations on $b$ in Fig. 6.

As is known, models with scale-dependent non-Gaussianities can account for the CMB anomalies as, for instance, the dipolar modulation [35,36,38,43,58]. Indeed, the model analyzed in Refs. [35,58] uses the non-Gaussianities to couple short- and long-scale modes in order to produce the hemispherical asymmetry. The presence of long (super-Hubble) modes of wave number $k_l$ can modulate the Bardeen power spectrum on short scales (inside the horizon). In such a model, the Universe remains isotropic, since the dependence on $k$ appears only due to the mode coupling. These models have the advantage, compared to Ref. [37], that there is no need for a large amplitude of the super-Hubble perturbations [58].

The scale dependence of the dipolar modulation roughly follows that of $f_{\rm NL}$ [58]. Thus, we expect $f_{\rm NL}$ to peak at $l < 64$. This provides a new source of observational constraint, which helps in constraining the parameters of non-Gaussian models. In Fig. 6, we show the behavior of $f_{\rm NL}$ for different values of $b$ and $c$. Varying the parameters $b$ and $c$ changes the position of the peak of $f_{\rm NL}$. Most recent observational results indicate the hemispherical asymmetry to be $A \approx 0.072$ for $l < 64$ [12,14]. For shorter scales, it reduces to $A < 0.0045$, for $l > 600$ [59,60]. The region of the parameter space which provides a peak for larger scales is preferred; otherwise, the asymmetry would be too high for smaller scales. That is particularly relevant for the quadrupole asymmetry [61–63]. It is also important to note that the spectral index is modulated in scenarios in the case that the non-Gaussianity is scale dependent [58], which presents another probe for $f_{\rm NL}$ and its effects.

Scale-dependent non-Gaussianity can also lead to bias in the cosmological parameter estimation based on the CMB, especially in the presence of a scale-dependent trispectrum [43]. Depending on the magnitude and scale dependence of the trispectrum, the bias on the spectral index $n_s$ can reach the order of $10^{-2}$, which is of the same order as the expected value of $\eta_\sigma$. Therefore, in different scenarios for non-Gaussian modulation, it is necessary to take into account all effects arising from the scale dependence from both the bispectrum and trispectrum, in order to rightly access the constraints on the system's parameter space.

So far, we have focused on building models in which the reconstruction procedure detailed in Sec. III B is well behaved, meaning that the point where $f_{\rm NL}$ changes sign is the closest possible between the ansatz and reconstructed solution. However, a discordance between the two solutions does not mean the choice of parameters is wrong. Such models may not agree with Eq. (29), but they still provide a scale dependence and magnitude for $f_{\rm NL}$ that fit observational constraints. Therefore, the theoretical predictions from the whole parameter space in Fig. 1 should be tested in comparison to observations.

## V. CONCLUSIONS

In the present work, we presented a procedure to reconstruct the curvaton potential from the non-Gaussianity parameter $f_{\rm NL}$. Assuming a slow-roll dynamic for the curvaton field, our procedure gives the curvaton potential that produces the desired $f_{\rm NL}$ [more precisely the $\sigma_{\rm osc}$, hence $f_{\rm NL}$; see Eq. (10)].

Planck's latest results indicate that cosmological perturbations at the pivot scale are highly Gaussian, $f_{\rm NL}^{\rm local} = -0.9 \pm 5.1$ [5]. That can be true for truly Gaussian fluctuations or for scale-dependent $f_{\rm NL}$. The latter satisfies the observational constraints if $f_{\rm NL}$ crosses zero close to the pivot scale but allows for higher values of non-Gaussianity for other scales.

We exemplified our method devising a curvaton model that results in a scale-dependent $f_{\rm NL}$ that changes sign twice and is bounded from above and below. In this manner, the non-Gaussianities have the desired features at the CMB pivot scale and avoid issues with the large scales probed by LSS surveys.

Scale-dependent non-Gaussianities are also known to be able to produce the hemispherical asymmetry observed in the CMB, in particular via non-Gaussian coupling between scalar modes [35]. Using the fact that our model predicts a peak in the $f_{\rm NL}$ parameter for scales larger than the pivot scale, we showed that it is possible to constrain the model using the asymmetry. If the peak is located towards higher values of $\ell$, constraints on the asymmetry are violated, which shows that the model should not predict a peak for $f_{\rm NL}$ located at $\ell > 64$. Note that our reconstructed model has the correct scale dependence for $f_{\rm NL}$—i.e., it grows towards larger scales/lower $\ell$. That is an advantage with respect to other curvaton models in the literature that commonly have the opposite scale dependence.

In Sec. IV A, we used $b = -20/e$ and $c = 216/e$ for the two parameters of the model in Eq. (29). As already mentioned, these values produce $f_{\rm NL}$ and $g_{\rm NL}$ larger than the latest Planck observational constraint, $f_{\rm NL} = -0.9 \pm 5.1$, $g_{\rm NL} = (-5.8 \pm 6.5) \times 10^4$. However, as Fig. 7 shows, a small increase in $c$ already drops $f_{\rm NL}$ and $g_{\rm NL}$ below the observational constraints (and this applies similarly to the parameter $b$). Therefore, the model on Fig. 7, with parameters $b = -20/e$ and $c = 248/e$, satisfies the Planck constraints [5]. It is worth noting that the Planck bounds for the nonlinearity parameters $f_{\rm NL}$ and $g_{\rm NL}$ are constructed considering a $f_{\rm NL}$ parameter that satisfies a power law [Eq. (14)] and a scale-independent $g_{\rm NL}$. That is not true for our model, so the available constraints for both parameters may not be directly applied.

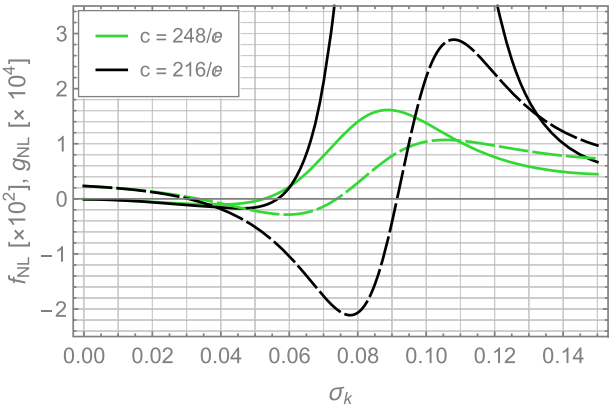


FIG. 7. Non-Gaussianity parameters $f_{\rm NL}$ (dashed lines) and $g_{\rm NL}$ (solid lines) for $b = -20/e$ and different values of $c$. Note that a change in $c$ causes $g_{\rm NL}$ to drop below the observational constraints—i.e., $g_{\rm NL} = (-5.8 \pm 6.5) \times 10^4$.

In order to adequately fit the parameters of the model with the observations, we need to consider additional effects present beyond first- and second-order scalar perturbations. In addition to the amplitude of perturbations and its spectral index (and subsequent running), in our scale-dependent curvaton scenario, the observational constraints also apply to the reheating scale (which is present in $r_{\rm dec}$, since it depends on $\Gamma$, which for the sudden decay approximation will have the same value as $H_{\rm reh}$). Thus, we have five free parameters: two from inflation, $H_k$ and $H_{\rm reh}$, and three from the parametrization, $a$, $b$, and $c$. The value of $H_k$ is especially important, since it enters in the computation of $\bar{\eta}_\sigma$. A numerical analysis is needed in order to precisely constrain the parameter space of the model. Our analytical computations do not consider the reheating process, which can slightly change scales for the crossings, as well as the amplitude of the nonlinearity parameters. We leave for a future work a detailed computation of all these effects and byproducts such as a modulation on the spectral index and a bias on cosmological parameter estimation.

## ACKNOWLEDGMENTS

We would like to thank Giovanni Marozzi for useful comments. The authors would like to thank and acknowledge financial support from the National Scientific and Technological Research Council (CNPq, Brazil). L. F. G. is supported in part by INFN under the program TAsP (*Theoretical Astroparticle Physics*). This study was financed in part by the Coordenação de Aperfeiçoamento de Pessoal de Nível Superior—Brasil (CAPES)—Finance Code 001.

[1] N. Aghanim *et al.* (Planck Collaboration), Astron. Astrophys. **641**, A1 (2020).
[2] N. Aghanim *et al.* (Planck Collaboration), Astron. Astrophys. **641**, A6 (2020).
[3] Y. Akrami *et al.* (Planck Collaboration), Astron. Astrophys. **641**, A10 (2020).
[4] J. Martin, C. Ringeval, R. Trotta, and V. Vennin, J. Cosmol. Astropart. Phys. 03 (2014) 039.
[5] Y. Akrami *et al.* (Planck Colloboration), Astron. Astrophys. **641**, A9 (2020).
[6] D. H. Lyth and A. Riotto, Phys. Rep. **314**, 1 (1999).
[7] P. Creminelli and M. Zaldarriaga, J. Cosmol. Astropart. Phys. 10 (2004) 006.
[8] G. Obied, H. Ooguri, L. Spodyneiko, and C. Vafa, arXiv: 1806.08362.
[9] P. Agrawal, G. Obied, P. J. Steinhardt, and C. Vafa, Phys. Lett. B **784**, 271 (2018).
[10] S. K. Garg and C. Krishnan, J. High Energy Phys. 11 (2019) 75.
[11] A. Bedroya, R. Brandenberger, M. Loverde, and C. Vafa, Phys. Rev. D **101**, 103502 (2020).
[12] P. A. R. Ade *et al.*, Astron. Astrophys. **594**, A16 (2016).
[13] C. J. Copi, D. Huterer, D. J. Schwarz, and G. D. Starkman, Adv. Astron. **2010**, 847541 (2010).
[14] D. J. Schwarz, C. J. Copi, D. Huterer, and G. D. Starkman, Classical Quan. Grav. **33**, 184001 (2016).
[15] L. F. Guimarães, F. T. Falciano, and G. Brando, Phys. Rev. D **99**, 103515 (2019).
[16] D. Wands, Phys. Rev. D **60**, 023507 (1999).
[17] F. Falciano, M. Lilley, and P. Peter, Phys. Rev. D **77**, 083513 (2008).
[18] N. Pinto-Neto, F. Falciano, R. Pereira, and E. Santini, Phys. Rev. D **86**, 063504 (2012).
[19] F. Falciano, N. Pinto-Neto, and S. D. Pinto Vitenti, Phys. Rev. D **87**, 103514 (2013).
[20] S. Vitenti, F. Falciano, and N. Pinto-Neto, Phys. Rev. D **87**, 103503 (2013).
[21] P. Peter, N. Pinto-Neto, and S. D. Vitenti, Phys. Rev. D **93**, 023520 (2016).
[22] P. Peter and N. Pinto-Neto, Phys. Rev. D **78**, 063506 (2008).
[23] R. Brandenberger and P. Peter, Found. Phys. **47**, 797 (2017).
[24] M. Lilley and P. Peter, C.R. Phys. **16**, 1038 (2015).
[25] R. H. Brandenberger, Classical Quan. Grav. **28**, 204005 (2011).
[26] S. Laliberte and R. Brandenberger, J. Cosmol. Astropart. Phys. 07 (2020) 046.
[27] R. Brandenberger and Z. Wang, Phys. Rev. D **101**, 063522 (2020).
[28] D. Wands, Multiple field inflation, in *Inflationary Cosmology*, edited by M. Lemoine, J. Martin, and P. Peter (Springer Berlin Heidelberg, Berlin, Heidelberg, 2007), pp. 275–304.
[29] A. Achúcarro and G. A. Palma, J. Cosmol. Astropart. Phys. 02 (2019) 041.
[30] M. Motaharfar, V. Kamali, and R. O. Ramos, Phys. Rev. D **99**, 063513 (2019).
[31] S. Das, Phys. Rev. D **99**, 083510 (2019).
[32] D. H. Lyth and D. Wands, Phys. Lett. B **524**, 5 (2002).
[33] D. H. Lyth, C. Ungarelli, and D. Wands, Phys. Rev. D **67**, 023503 (2003).
[34] V. Vennin, K. Koyama, and D. Wands, J. Cosmol. Astropart. Phys. 11 (2015) 008.
[35] F. Schmidt and L. Hui, Phys. Rev. Lett. **110**, 011301 (2013).
[36] C. T. Byrnes and E. R. Tarrant, J. Cosmol. Astropart. Phys. 07 (2015) 007.
[37] C. T. Byrnes, D. Regan, D. Seery, and E. R. M. Tarrant, Phys. Rev. D **93**, 123003 (2016).
[38] C. T. Byrnes, D. Regan, D. Seery, and E. R. Tarrant, J. Cosmol. Astropart. Phys. 06 (**2016**) 025.
[39] Z. Kenton, D. J. Mulryne, and S. Thomas, Phys. Rev. D **92**, 023505 (2015).
[40] Q.-G. Huang, J. Cosmol. Astropart. Phys. 11 (2008) 005.
[41] K. Enqvist, S. Nurmi, O. Taanila, and T. Takahashi, J. Cosmol. Astropart. Phys. 04 (**2010**) 009.
[42] C. T. Byrnes, K. Enqvist, S. Nurmi, and T. Takahashi, J. Cosmol. Astropart. Phys. 11 (**2011**) 011.
[43] S. Adhikari, A.-S. Deutsch, and S. Shandera, Phys. Rev. D **98**, 023520 (2018).
[44] F. K. Hansen, T. Trombetti, N. Bartolo, U. Natale, M. Liguori, A. J. Banday, and K. M. Górski, Astron. Astrophys. **626**, A13 (2019).
[45] D. Langlois and F. Vernizzi, Phys. Rev. D **70**, 063522 (2004).
[46] K. Ichikawa, T. Suyama, T. Takahashi, and M. Yamaguchi, Phys. Rev. D **78**, 023513 (2008).
[47] C. T. Byrnes, M. Cortês, and A. R. Liddle, Phys. Rev. D **90**, 023523 (2014).
[48] M. Kawasaki, T. Kobayashi, and F. Takahashi, Phys. Rev. D **84**, 123506 (2011).
[49] J. Meyers and E. R. M. Tarrant, Phys. Rev. D **89**, 063535 (2014).
[50] S. Mollerach, Phys. Rev. D **42**, 313 (1990).
[51] D. H. Lyth and Y. Rodríguez, Phys. Rev. Lett. **95**, 121302 (2005).
[52] A. Linde, Phys. Lett. **129B**, 177 (1983).
[53] M. Sasaki, J. Väliviita, and D. Wands, Phys. Rev. D **74**, 103003 (2006).
[54] K. Enqvist, S. Nurmi, G. Rigopoulos, O. Taanila, and T. Takahashi, J. Cosmol. Astropart. Phys. 11 (2009) 003.
[55] E. Sefusatti, M. Liguori, A. P. Yadav, M. G. Jackson, and E. Pajer, J. Cosmol. Astropart. Phys. 12 (2009) 022.
[56] C. T. Byrnes, S. Nurmi, G. Tasinato, and D. Wands, J. Cosmol. Astropart. Phys. 02 (**2010**) 034.
[57] K. Enqvist, D. J. Mulryne, and S. Nurmi, J. Cosmol. Astropart. Phys. 05 (2015) 010.
[58] S. Adhikari, S. Shandera, and A. L. Erickcek, Phys. Rev. D **93**, 023524 (2016).
[59] S. Flender and S. Hotchkiss, J. Cosmol. Astropart. Phys. 09 (2013) 033.
[60] M. Quartin and A. Notari, J. Cosmol. Astropart. Phys. 01 (2015) 008.
[61] C. M. Hirata, J. Cosmol. Astropart. Phys. 09 (2009) 011.
[62] S. Kanno, M. Sasaki, and T. Tanaka, Prog. Theor. Exp. Phys. **2013**, 111E01 (2013).
[63] A. Marcos-Caballero and E. Martínez-González, J. Cosmol. Astropart. Phys. 10 (2019) 053.